Airborne IP: examples from the Mount Milligan deposit, Canada, and the Amakinskaya kimberlite pipe, Russia

Andrea Viezzoli[1] Vlad Kaminski[1,2]

[1]Aarhus Geophysics, ApS, Lollandsgade 52, Aarhus, DK-8000, Denmark.
[2]Corresponding author. Email: vlad.kaminski@aarhusgeo.com

Abstract.   There have been multiple occurrences in the literature in the past several years of what has been referred to as the induced polarisation (IP) effect in airborne time domain electromagnetic (TDEM) data. This phenomenon is known to be responsible for incorrect inversion modelling of electrical resistivity, lower interpreted depth of investigation (DOI) and lost information about chargeability of the subsurface and other valuable parameters. Historically, there have been many suggestions to account for the IP effect using the Cole-Cole model. It has been previously demonstrated that the Cole-Cole model can be effective in modelling synthetic TDEM transients. In the current paper we show the possibility of extracting IP information from airborne TDEM data using this same concept, including inverse modelling of chargeability from TDEM data collected by VTEM, with field examples from Canada (Mt Milligan deposit) and Russia (Amakinskaya kimberlite pipe).

Key words: airborne EM, airborne IP, inversion, kimberlite, mineral exploration, modelling, porphyry.

Introduction

The induced polarisation (IP) effect in time domain electromagnetic (TDEM) data can be observed in coincident-loop TDEM systems and is manifested as abnormally quick decay, which sometimes causes the measured voltage values in the receiver coil to demonstrate negative values. This phenomenon can significantly alter the shape of the transients, and therefore, mislead the interpretation to recover false structures with incorrect conductivity-thickness parameters. IP effect has been recognised in the ground-based TDEM, including work done by Kozhevnikov and Antonov (2007), Antonov and Shein (2008), Kozhevnikov and Antonov (2009) and Kamenetsky et al. (2014). Nonetheless, for a long time it has been standard practice within the geophysical community to neglect this effect in airborne data and eliminate any negative values when inverting the TDEM data.

There has been a recent and increasing interest in the IP effect in airborne data, as it carries potential for recovery of the Cole-Cole parameters (Cole and Cole, 1942), including chargeability information, which can be extracted from the airborne EM data, along with other Cole-Cole parameters. These recent attempts include work done by Kratzer and Macnae (2012), where VTEM results acquired in Africa were processed to provide a chargeability distribution model. Other preliminary synthetic and field results have been demonstrated in Kaminski et al. (2015), Kwan et al. (2015a), Viezzoli et al. (2013) and Viezzoli et al. (2015a). In this paper, we focus on the practical implementation of these algorithms and show some results from field data acquired in western Canada (Mt Milligan porphyry copper-gold deposit), as well as in northern Russia (Amakinskaya kimberlite pipe).

The extraction of Cole-Cole parameters is handled by means of laterally constrained inversion (LCI) or spatially constrained inversion (SCI) (Viezzoli et al., 2008; Fiandaca et al., 2012).

The difference between these two codes is in the construction of the model objective function, with LCI inversion designed to invert with consideration of two constraints (vertical and in the direction of the flight), while the SCI concept is effectively a quasi three-dimensional (3D) code, capable of using 3D constraints along and across the flight lines. Both inversions (LCI and SCI) use similar forward mapping kernel, based on one-dimensional (1D) considerations, in which the complex resistivity (dispersive model) is generally governed by Equation 1:

$$\zeta(\omega) = \rho \left[1 - \frac{m_0}{10^3} \left(1 - \frac{1}{1 + (i\omega\tau)^c} \right) \right] \qquad (1)$$

where $\zeta(\omega)$ is the complex frequency dependent resistivity, ρ is the DC resistivity, m_0 is the chargeability, τ is the relaxation time and c is the frequency parameter (Cole and Cole, 1942). The inversion algorithm, modified as per Fiandaca et al. (2012), provides combined estimates of all four parameters from Equation 1 in two modes described above (LCI and SCI).

The inversions are subject to heavy regularisation and user-defined constraints. There are, however, very notable correlations between the extractions of chargeability from airborne data with chargeability sections derived from ground IP surveys, as shown in the first example. Furthermore, recovery of frequency parameter c along with relaxation time τ can also carry valuable geological information, which cannot be derived from any other type of geophysical data.

Example 1: Mount Milligan, Canada

Mt Milligan is a large Cu-Au porphyry deposit situated in central British Columbia (Figure 1). Geologically, the Mt Milligan deposit is a mineralised zone within a porphyrite-monzonite stock (MBX), hosted within andesites and
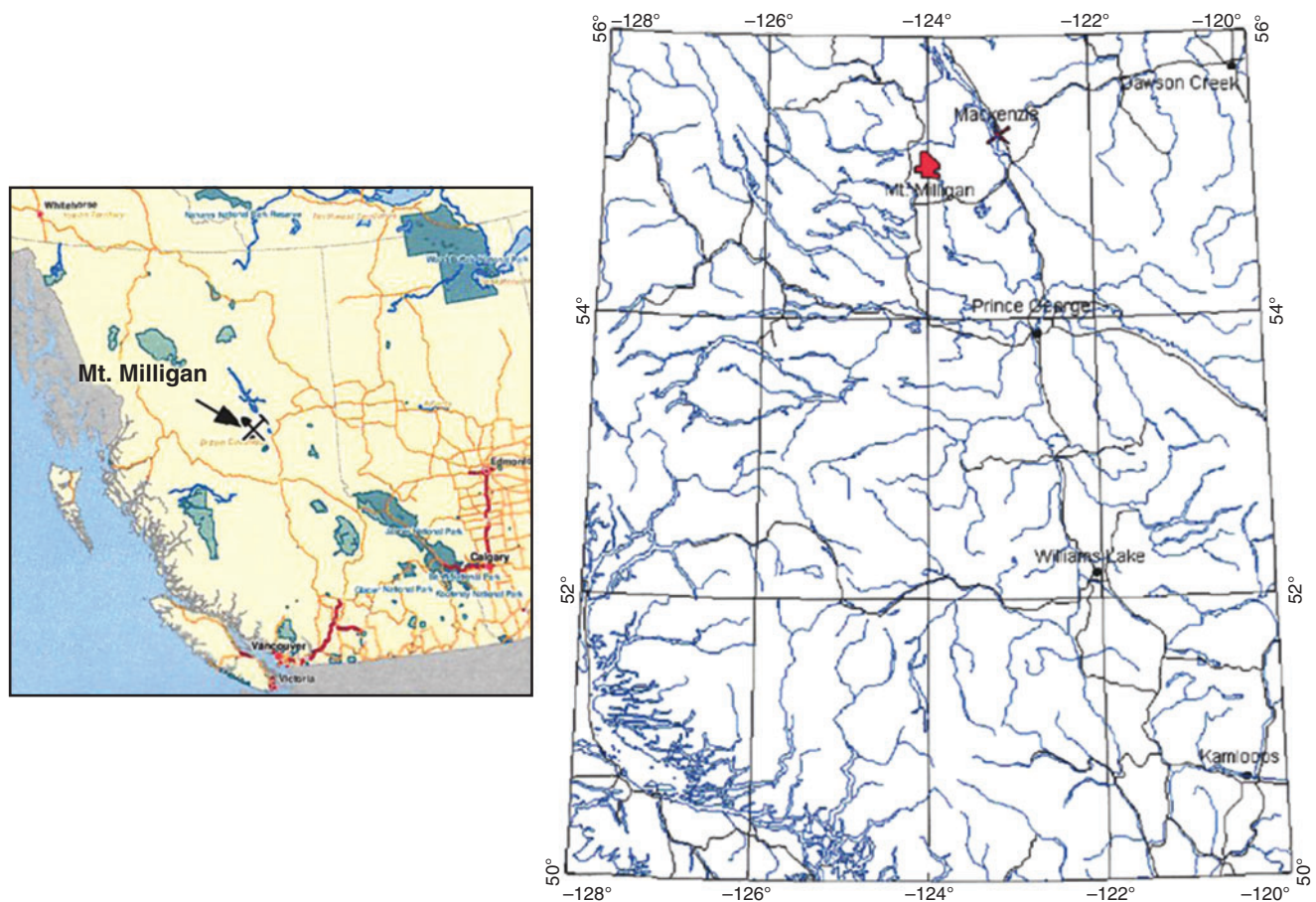
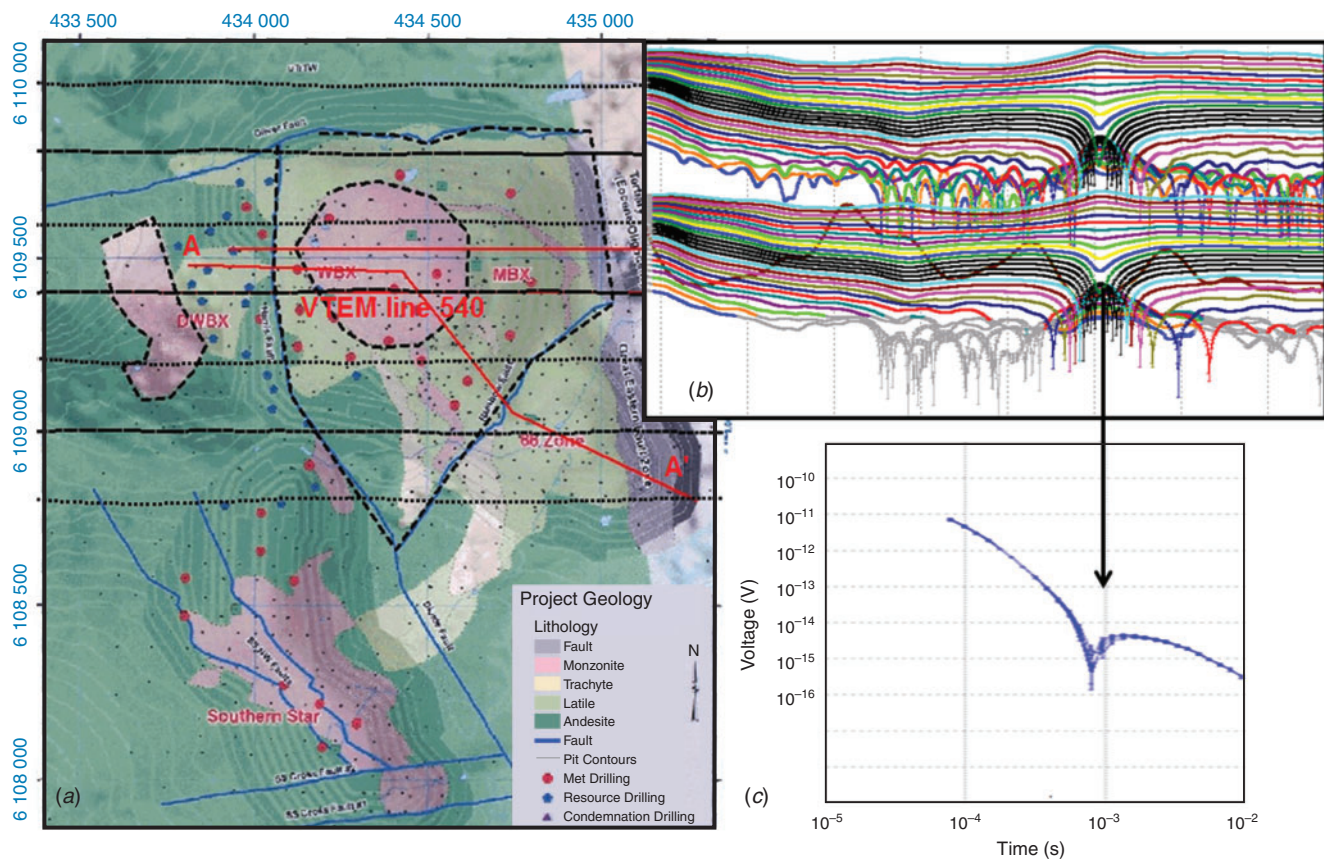**Fig. 1.**   Location and bedrock geology of Mt Milligan deposit, Canada.

Fig. 2.   (*a*) Bedrock geology of Mt Milligan deposit; (*b*) visible IP effect in VTEM data (flight line 540); (*c*) IP effect in individual transients.
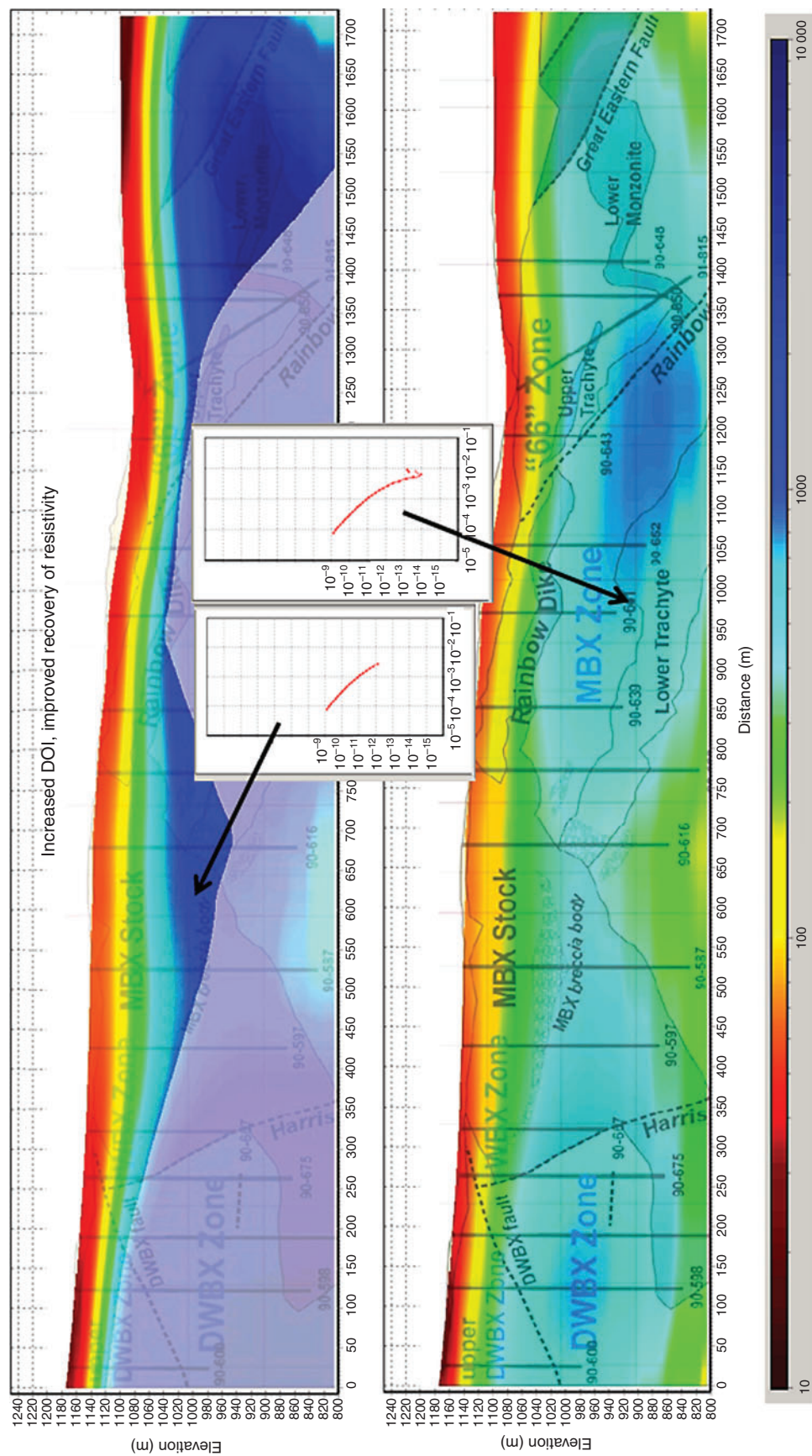
Fig. 3. Top: non-IP inversion of VTEM data over Mt Milligan deposit; bottom: IP inversion (Cole-Cole model) over Mt Milligan deposit.

volcanites of the Takla Group (DeLong et al., 1991). There are two types of alteration present in the Mt Milligan deposit: potassic and propylitic. These alterations are responsible for different physical properties. Chargeability is a crucial property for the Mt Milligan deposit, as it may be indicative of the gold-bearing mineralisation, which is

otherwise undetectable due to poor electrical conductivity of the mineralisation (Oldenburg et al., 1997).

In 2008, the deposit was surveyed by the VTEM system at the request of Geoscience BC and showed significant IP effect in the data (Figure 2). Previous attempts to invert these data include Schwarzbach et al. (2013), which was done
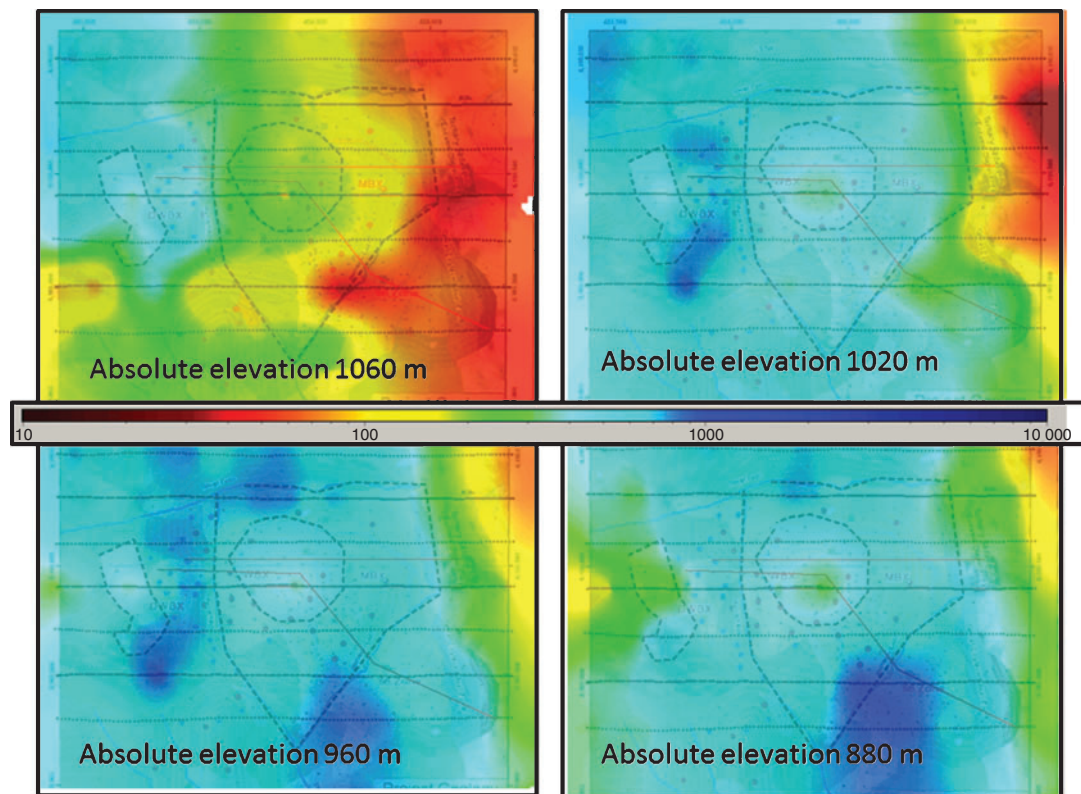
Fig. 4.   Series of resistivity depth slices (Ωm) generated from an SCI quasi-3D inversion 3D volume interpolation.
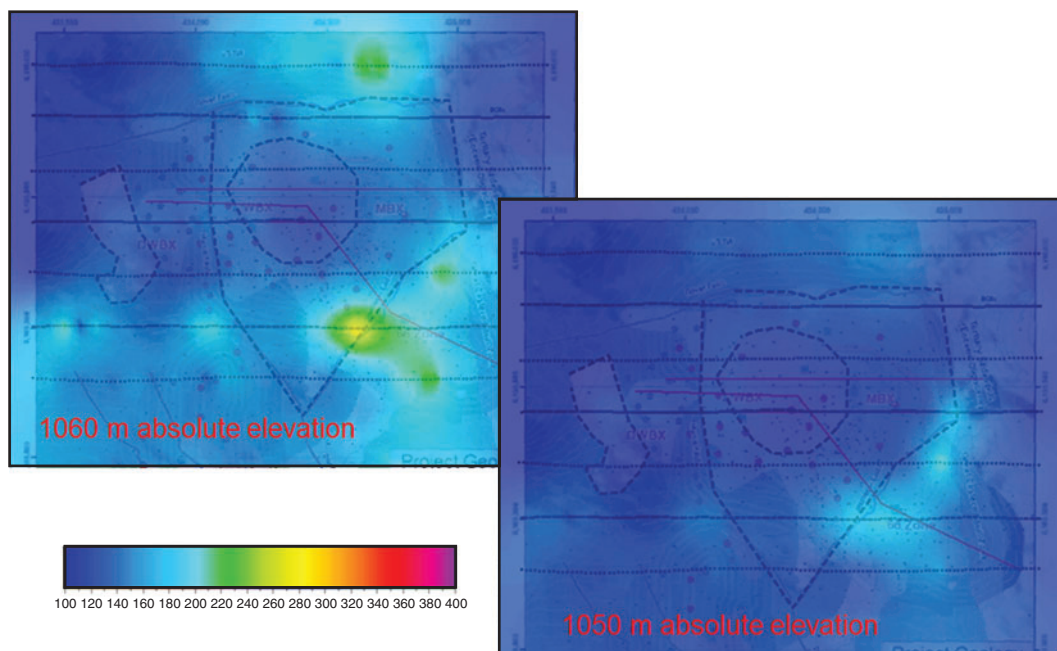
Fig. 5.   Chargeability (mV/V) depth slices produced from interpolated results of Cole-Cole SCI inversion 3D volume interpolation.
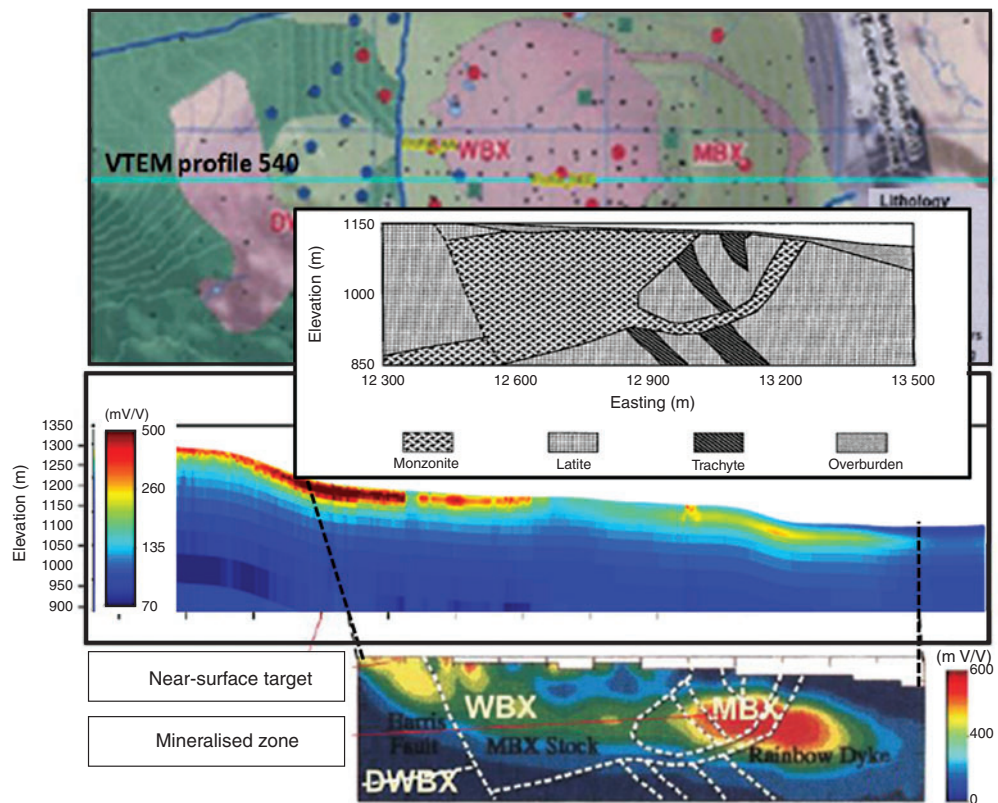
Fig. 6.   Comparison between ground IP chargeability and chargeability recovered from TDEM data.
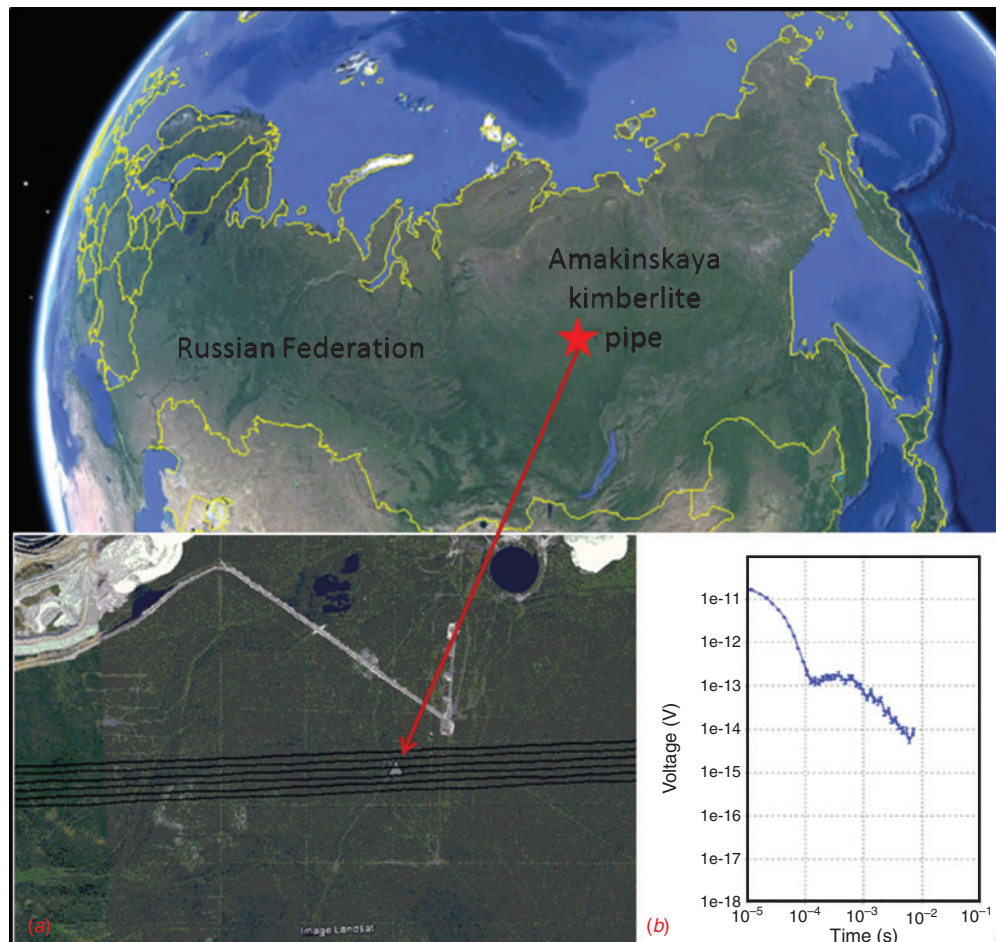

Fig. 7.   Location of Amakinskaya kimberlite pipe, north-eastern Russia. (*a*) VTEM flight lines shown over Landsat image; (*b*) IP effect measured over the kimberlite, shown in VTEM individual transients.

without consideration of the IP effect. Kwan et al. (2015*b*) have recently contributed to analysis of the IP effect in these VTEM data.

For the purpose of current study, the VTEM data were inverted using the SCI approach. A first attempt was made without the consideration of the IP effect, and then the data were inverted in IP mode. Figure 3 shows the comparison of resistivity depth sections with and without modelling of the IP effect, both clipped to interpreted depth of investigation (DOI). As can be seen in Figure 3, the 'MBX' marks the extent of the monzonite stock, which along with Rainbow Dike, are showing the highest grades of gold concentration in the deposit (DeLong et al., 1991). In this figure there is significant improvement in DOI due to modelling of the IP effect. Furthermore, the improved resistivity section (lower section) shows good correlation with the geology (e.g. the resistive response of DWBX and MBX zones, the conductive signature of overburden, WBX, and '66' zones).

The results of the SCI inversion in IP mode were interpolated to populate a 3D volume. The 3D volume was then sliced in XY direction, generating resistivity and chargeability depth slices, plotted over the bedrock geology (Figures 4 and 5). The recovered chargeability was further investigated and compared to the chargeability section recovered from the ground IP survey (Oldenburg et al., 1997). This comparison is shown in Figure 6. The profile adapted from Oldenburg et al. (1997) is nearly coincident with VTEM flight line 540; however, the actual ground IP data was unavailable to us, and therefore, the comparison is based on visual inspection of the results.

Example 2: Amakinskaya kimberlite pipe, Russia

The second example shows a study carried out over the Amakinskaya kimberlite pipe situated in Yakutia (north-eastern Russia, Figure 7).
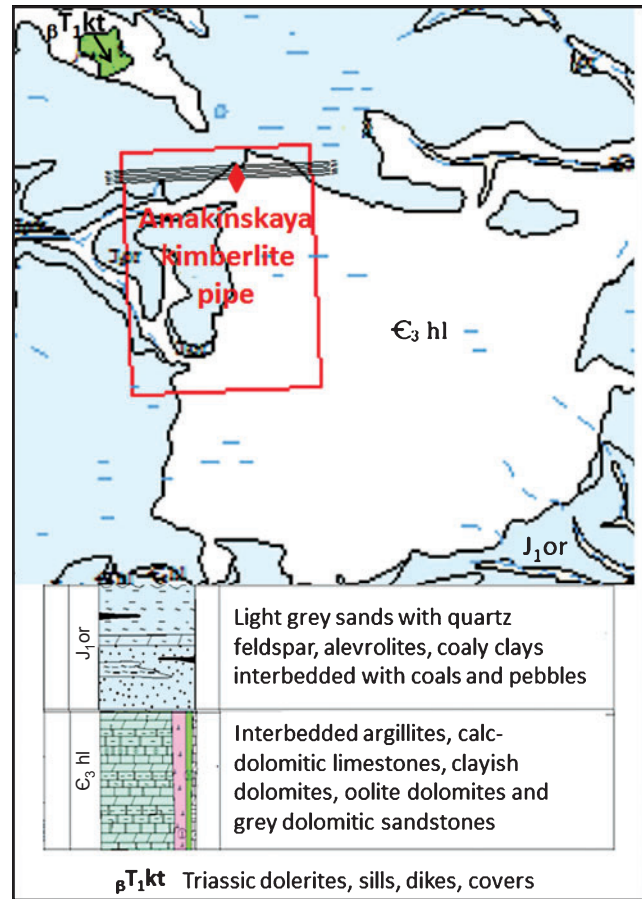

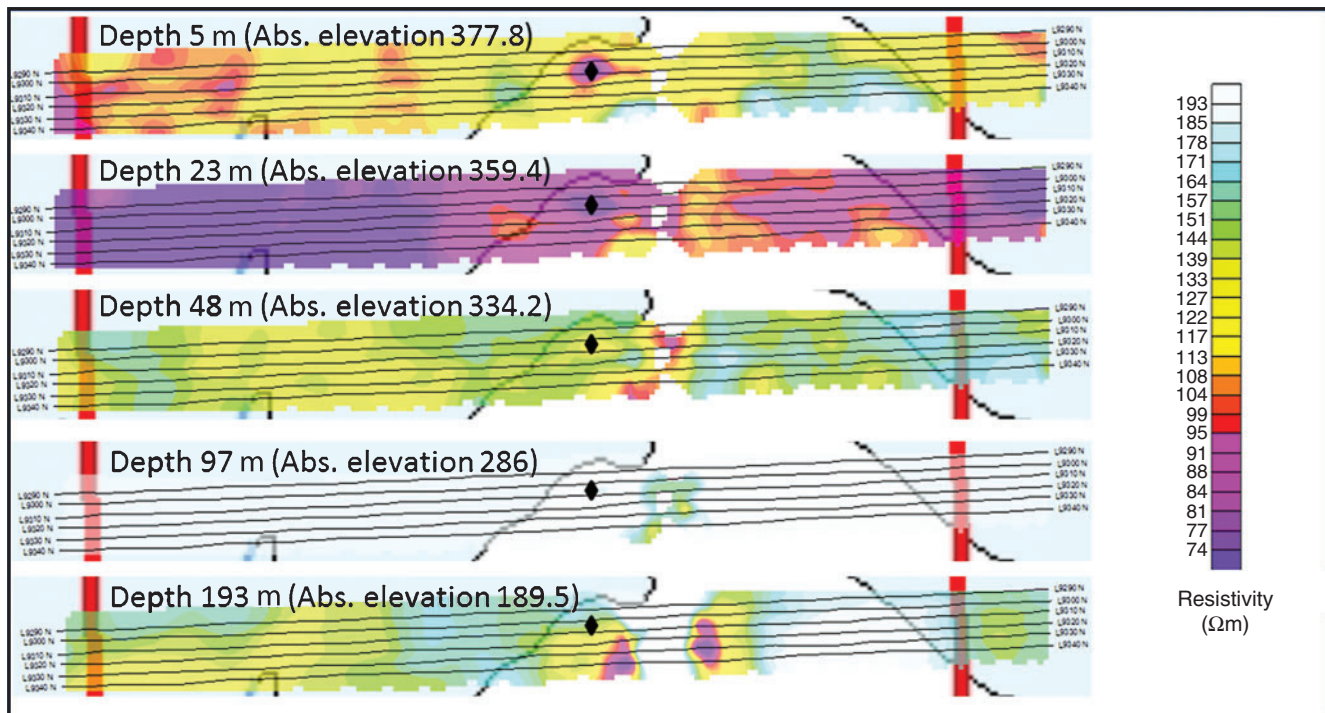**Fig. 8.**   Geological setting of the area under study.

Fig. 9.   3D distribution of electrical resistivity recovered by SCI inversion with IP modelling over Amakinskaya kimberlite pipe, shown as series of depth slices.

From the geological standpoint, the area surrounding the Amakinskaya kimberlite pipe belongs to a sedimentary basin with widespread outcrops of clays and alevrolites of Jurassic age (J_1or), which unconformably overlay the Cambrian limestone complex ($Є_3$hl). Triassic basalts ($βT_1$kt) are also widespread in the area, especially to the north of the pipe (Figure 8).

The Amakinskaya kimberlite pipe shows a great deal of anisotropy in the vertical direction, shifting from weathered, clayish upper facies affected by permafrost, to consolidated hard kimberlite below a depth of 30 m. This is obviously reflected in the physical properties of the kimberlite. Resistivity and chargeability changes with depth, showing lowering resistivity and increasing chargeability values in the upper facies of the kimberlite, while magnetic susceptibility increases with depth as the kimberlite consolidates (Bondarenko and Zinchuk, 2004).

The airborne survey was flown in late 2014 using a VTEM system and the data were seriously affected by the IP effect (Figure 7b). It should be noted, however, that the IP effect over the kimberlite, although evident in the transients, does not result in negative voltage measurements and therefore may not be instantly obvious in the data space at first glance. One of the analyses of these data for IP effects includes Kwan et al. (2015a). In addition to strong IP effect, which made conventional inversion challenging, there was a strong electrified industrial infrastructure situated just 200 m east of the Amakinskaya pipe, seriously affecting both EM and magnetic data. This cultural noise had to be removed from all datasets in order to proceed further with inverting the data.

In general, the IP effect may be indicative of the clay alteration, which in turn, may be present in upper (weathered)
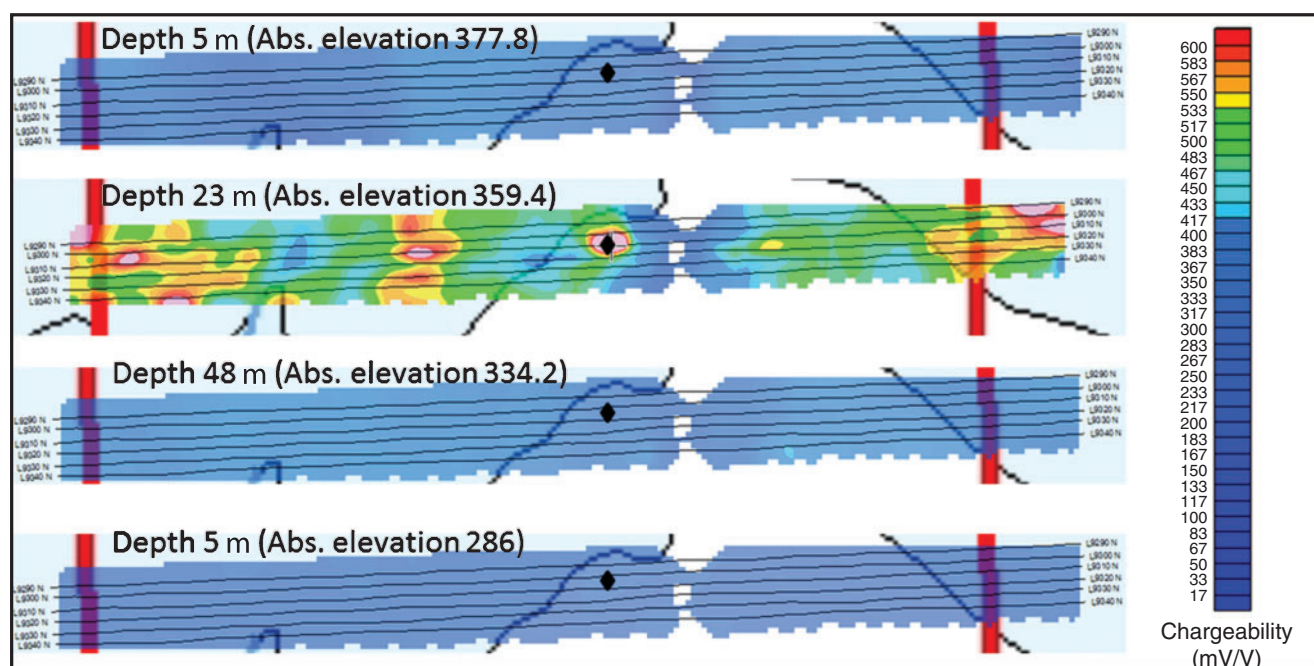

Fig. 10. 3D distribution of chargeability recovered by SCI inversion with IP modelling over Amakinskaya kimberlite pipe, shown as series of depth slices.
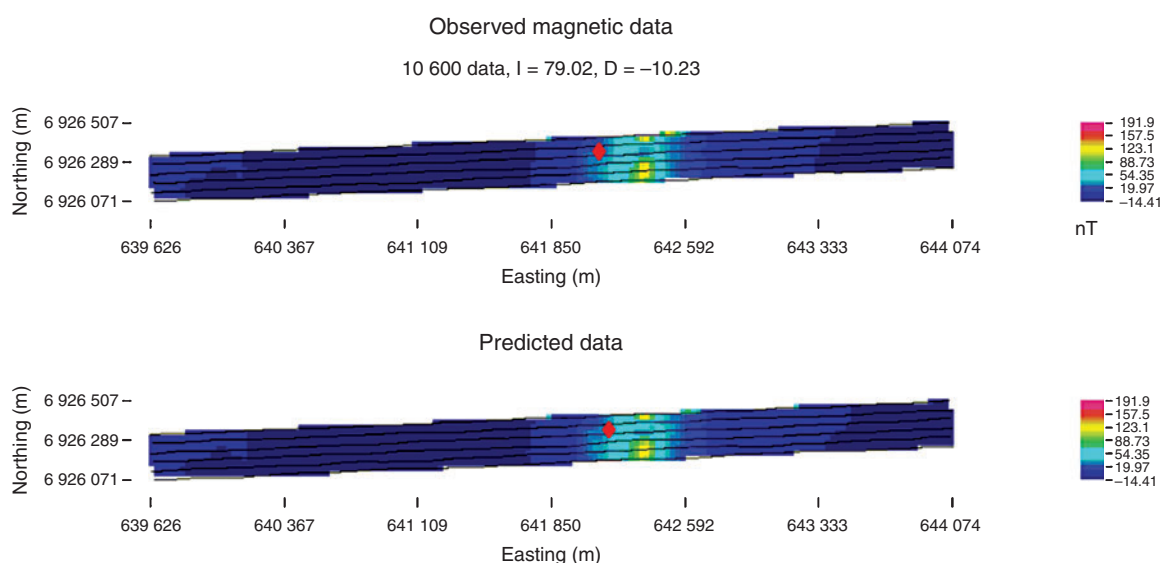

Fig. 11. Observed versus predicted magnetic data for the 3D inversion over Amakinskaya kimberlite pipe.
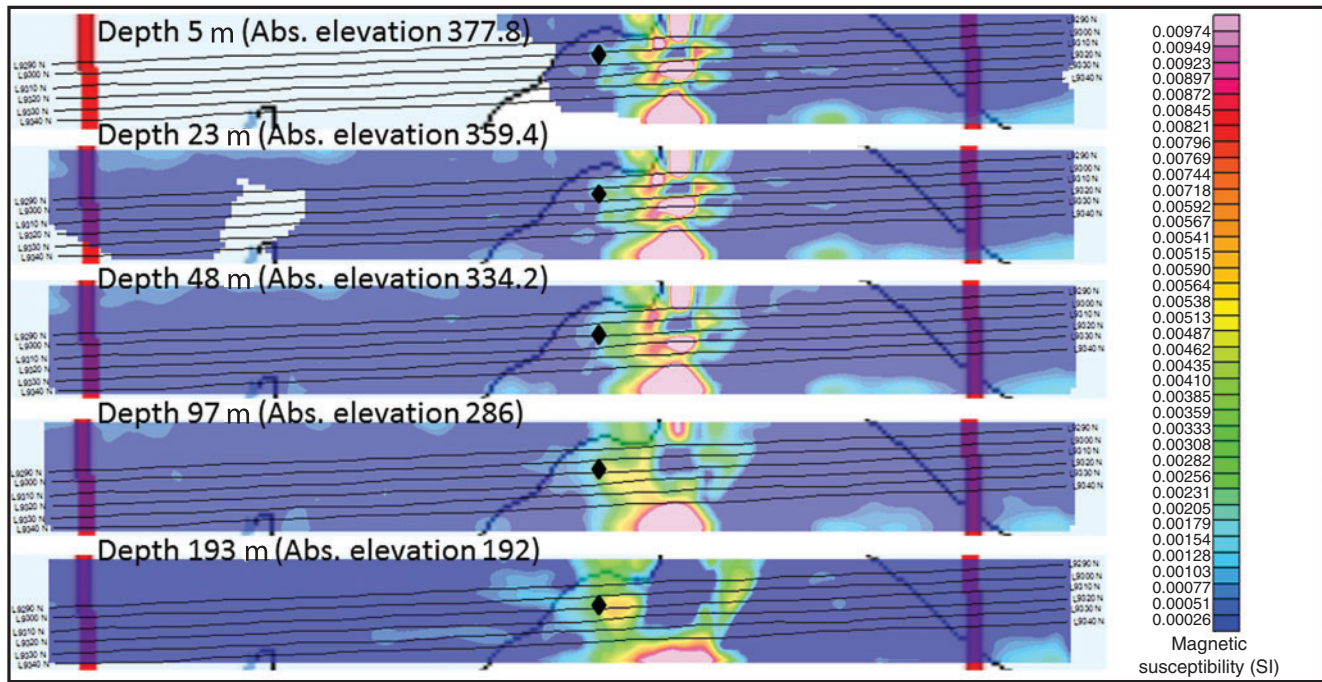
Fig. 12. Results of 3D magnetic inversion over Amakinskaya kimberlite pipe, plotted as series of depth slices.

facies of a kimberlite (Kaminski and Oldenburg, 2012). Interpretation of the IP effect over kimberlites for ground TDEM surveys has been previously described in the literature (Kamenetsky et al., 2014), and becomes increasingly attractive in cases with airborne TDEM datasets as it allows extraction of chargeability, along with other valuable parameters, such as relaxation time (τ) and frequency parameter (c).

In this particular case study, there is a thick layer of permafrost present, which greatly contributes to the IP effect in the TDEM data, along with the presence of clay material in the weathered upper part of the kimberlite. However, the electrical processes in the permafrost result in a higher range of frequency parameter c than those processes in the fine-grained clay particles, which result in lower c values. Similar observations were made by Kamenetsky et al. (2014) over other kimberlite pipes from Yakutia, Russia, which are situated within 200 km from the Amakinskaya pipe and where permafrost is also widely spread.

Therefore, in order to distinguish between the two types of IP effect it will be important to implement the frequency parameter analysis. Some preliminary results from this area were shown in Viezzoli et al. (2015*b*). Although frequency parameter analysis is omitted in this current study, we believe that such an approach carries great potential for interpretation of IP-affected airborne data in similar cases.

As a result of SCI inversion approach with IP modelling, all four Cole-Cole parameters were extracted. The target misfits of the inversions were achieved, producing distributions of Cole-Cole parameters, which were further interpolated to populate 3D volumes. The distributions of electrical resistivity and chargeability with depth are shown in Figures 9 and 10.

In addition to the SCI inversion performed on TDEM data, a 3D magnetic inversion was carried out over the Amakinskaya pipe. The pipe is reflected in the total magnetic intensity (TMI). The 3D magnetic inversion was carried out over 10 600 IGRF (International Geomagnetic Reference Field)-corrected magnetic data. The 3D volume was discretised onto a $10 \times 10 \times 5$ m mesh, producing a model of $457 \times$
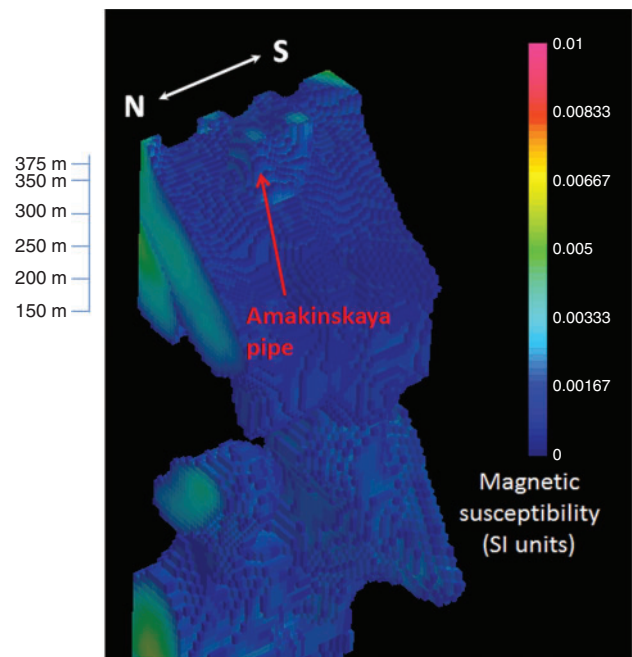

Fig. 13. A voxel model with 3D magnetic inversion results over the Amakinskaya kimberlite pipe.

56×125 voxels. The convergence was achieved in seven iterations, reaching the target misfit of 1.8 nT (Figure 11). The results of 3D magnetic inversion were plotted as a series of depth slices similarly to the results of SCI inversion (Figure 12). Finally, these results are shown in a 3D volume voxel model (Figure 13).

As it can be seen in Figure 14, the 3D model suggests that the body of the kimberlite is split into two morphological units close to the surface, which is indeed consistent with the known morphology of Amakinskaya pipe (Bondarenko and Zinchuk, 2004).
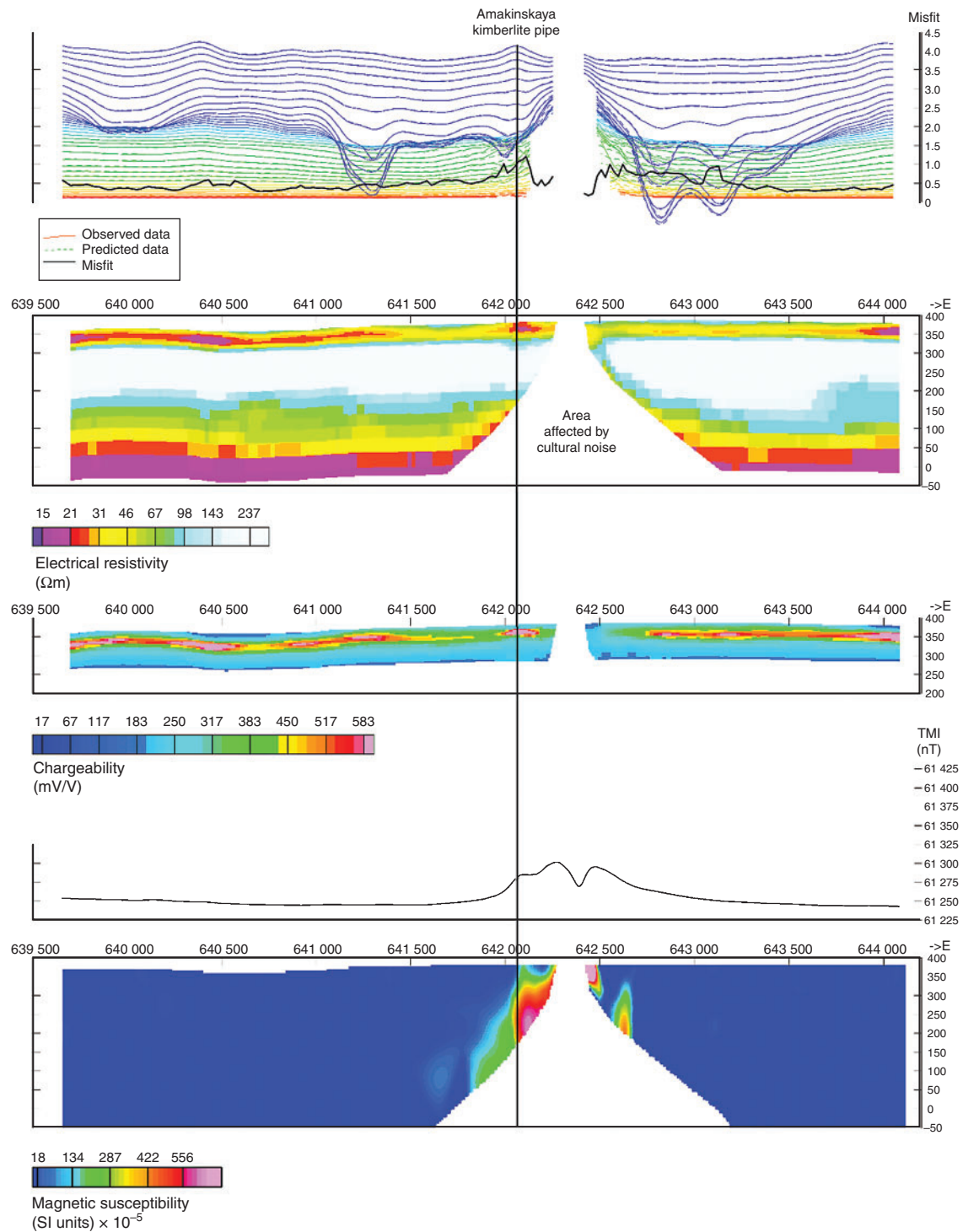
Fig. 14.   Compilation of inversion results over VTEM flight line 9310.

Overall, the results of the inversions allow clear differentiation between the kimberlite and the host rock. The results are shown in Figure 14 as a compilation of all inversion results, interpolated along VTEM flight line 9310 and shown as a depth section of electrical resistivity, chargeability and magnetic susceptibility.

Conclusions

By applying the Cole-Cole model in the inversions of TDEM data, we demonstrate the ability to map the 3D distribution of physical parameters in the subsurface, which brings new value to mineral exploration. In our first example, we show improved resistivity imaging by virtue of accounting for the IP effect in the TDEM data, as well as capability to map chargeability, which is, to an extent, in agreement with ground IP survey results. Not only does the IP inversion bring greater DOI and improved recovery of electrical resistivity, but in the case of the Mt Milligan deposit, the ability to extract chargeability plays a crucial role, since the deposit is electrically resistive and chargeability becomes a primary quality in overall detectability of the deposit (Oldenburg et al., 1997).

In our second case study, we have used a complex approach with the successful result of delineating Amakinskaya kimberlite pipe in all three physical properties, despite the presence of very strong industrial noise only 200 m east of the exploration target. It should be noted, however, that the greatest visibility of the pipe is evident in recovered chargeability, which was made possible by virtue of the SCI inversion with Cole-Cole modelling. In general, a similar complex approach is suggested for future usage as a desirable interpretation method for kimberlite exploration in other parts of the world. Special attention should be paid to the interpretation of other Cole-Cole parameters, such as relaxation time (τ) and frequency parameter (c), as they are carrying valuable information, which may be helpful in interpretation of the IP-affected data.

Acknowledgements

References

Antonov, E., and Shein, A., 2008, Improving inversion quality of IP-affected TDEM data: *Russian Geology and Geophysics*, **49**, 790–802. doi:10.1016/j.rgg.2008.01.008

Bondarenko, A., and Zinchuk, M. 2004, Petrophysics and characteristics of host rocks; environmental aspects of kimberlite exploration: Technical Report, TSNIGRI, Mirny, Russia.

Cole, K. S., and Cole, R. H., 1942, Dispersion and absorption in dielectrics: *Journal of Chemical Physics*, **9**, 341–351. doi:10.1063/1.1750906

DeLong, R. C., Godwin, E. I., Harris, M. W. H., Caira, N. M., and Rebagliati, C. M., 1991, Geology and alteration at the Mt Milligan Gold-Porphyry Deposit, Central British Columbia: British Columbia Ministry of Energy, Mines, and Petroleum Resources – Geological Survey Branch, Paper, 199–205.

Fiandaca, G., Auken, E., Christiansen, A. V., and Gazoty, A., 2012, Time-domain-induced polarization: full-decay forward modelling and 1D laterally constrained inversion of Cole-Cole parameters: *Geophysics*, **77**, E213–E225. doi:10.1190/geo2011-0217.1

Kamenetsky, F., Trigubovich, G., and Chernyshev, A. 2014, *Three lectures on geological medium induced polarization*: Ludwig-Maximilian University of Munich, 43–54.

Kaminski, V., and Oldenburg, D., 2012, The geophysical study of Drybones kimberlite using 3D time domain EM inversion and 3D ZTEM inversion algorithms: 22nd ASEG International Geophysical Conference and Exhibition, Expanded Abstracts, 1–4.

Kaminski, V., Viezzoli, A., Menghini, A., and Fiandaca, G., 2015, Case studies of modelling IP effect in AEM data: EAGE 21st European Meeting of Environmental and Engineering Geophysics, Expanded Abstracts, 1–4.

Kozhevnikov, N., and Antonov, E., 2007, Inversion of IP-affected TEM data: a numerical experiment with a model of a uniform polarizing half-space: *Geofizika*, **1**, 42–50.

Kozhevnikov, N., and Antonov, E., 2009, Joint inversion of IP-affected TEM data: *Russian Geology and Geophysics*, **50**, 136–142. doi:10.1016/j.rgg.2008.06.021

Kratzer, T., and Macnae, J., 2012, Induced polarization in airborne EM: *Geophysics*, **77**, E317–E327. doi:10.1190/geo2011-0492.1

Kwan, K., Prikhodko, A., and Legault, J., 2015a, Airborne inductively induced polarization effects in and their removal from the VTEM data from Mirny, Russia: 85th Annual International Meeting, SEG, Expanded Abstracts, 1–4.

Kwan, K., Prikhodko, A., and Legault, J., 2015b, Airborne inductive induced polarization chargeability mapping of VTEM data: 22nd ASEG International Geophysical Conference and Exhibition, Expanded Abstracts, 1–4.

Oldenburg, D. W., Li, Y., and Ellis, R. G., 1997, Inversion of geophysical data over a copper gold porphyry deposit: a case history for Mt. Milligan: *Geophysics*, **62**, 1419–1431. doi:10.1190/1.1444246

Schwarzbach, C., Holtham, E., and Haber, E., 2013, 3D inversion of large-scale time domain electromagnetic data: 23rd ASEG-PESA International Geophysical Conference and Exhibition, Expanded Abstracts, 1–4.

Viezzoli, A., Christiansen, A. V., Auken, E., and Sorensen, K., 2008, Quasi-3D modelling of airborne TEM data by spatially constrained inversion: *Geophysics*, **73**, F105–F113. doi:10.1190/1.2895521

Viezzoli, A., Fiandaca, G., Auken, E., Christiansen, A., Sergio, S., 2013, Constrained inversion of IP parameters from airborne EM data: 23rd ASEG-PESA International Geophysical Conference and Exhibition, Expanded Abstracts, 1–5.

Viezzoli, A., Kaminski, V., Ley-Cooper, Y., Hardy, L., and Fiandaca, G., 2015a, Improving modelling of AEM data affected by IP, two case studies: 24th ASEG-PESA International Geophysical Conference and Exhibition, Expanded Abstracts, 1–5.

Viezzoli, A., Kaminski, V., and Goncharov, E., 2015b, Airborne IP: examples from gold and kimberlite exploration: 14th SAGA Biennial Technical Meeting and Exhibition, Expanded Abstracts, 1–4.